High-Temperature Steam Oxidation Study of Irradiated FeCrAl Defueled Specimens

Y. Yan, J. Harp, A. Le Coq, C. Massey, K. Linton

Oak Ridge National Laboratory, Oak Ridge, TN 37831, USA

Abstract

Post irradiation examinations (PIE) were performed on irradiated iron-chromium-aluminum (FeCrAl) specimens. These FeCrAl specimens were fabricated at the US Department of Energy's Oak Ridge National Laboratory (ORNL). The experimental setup involved subjecting FeCrAl cladding, along with UO_2 pellets, to irradiation in the Idaho National Laboratory Advanced Test Reactor (ATR). In parallel, the FeCrAl alloy tubing without UO_2 pellets was irradiated at ORNL's High Flux Isotope Reactor (HFIR). After irradiation, the ATR-irradiated rodlet was transported to an ORNL hot cell, where it was sectioned into multiple samples for the PIE and severe-accident testing. The sectioning process revealed that the fuel was not bonded to the cladding and could be easily detached from sectioned cladding slices. Microstructural analysis of the fuel cross sections demonstrated no significant interaction between the fuel and the cladding. Additionally, high-temperature steam oxidation tests on defueled cladding segments showed minimal oxygen uptake even at 1200°C. The ATR-irradiated specimens began to exhibit signs of enhanced oxidation upon reaching a temperature of 1300°C. Furthermore, enhanced oxidation was observed on the inner surface of the ATR-irradiated FeCrAl specimen, which had been subjected to 1300°C for a duration of 1 min. By contrast, high-temperature steam oxidation experiments indicated that the HFIR-irradiated FeCrAl cladding provided good thermal stability when exposed to 1300°C for up to 4 h. Comparative analysis encompassing the oxidation behavior of the ATR-irradiated fueled FeCrAl, HFIR-irradiated unfueled FeCrAl, and unirradiated FeCrAl suggests that the fuel–cladding interaction, although not visible via standard microscale electron microscopy measurements, may accelerate the deterioration of FeCrAl cladding in beyond-design-basis accident scenarios.

1. INTRODUCTION

The 2011 Fukushima-Daiichi accident motivates research on accident-tolerant nuclear fuels (ATFs) [1,2]. Enhanced ATF materials are being developed for deployment in commercial light-water reactors through a collaboration among the US Department of Energy Office of Nuclear Energy (DOE NE) Advanced Fuels Campaign (AFC) and US fuel vendors. These ATF cladding materials are designed specifically to provide additional margins of safety in the event of a postulated beyond-design-basis accident such as that experienced at Fukushima-Daiichi. In this scenario, cladding materials would be subjected to high-temperature steam (near or exceeding 1200°C) for extended periods of time. At these temperatures, the exothermic reaction between Zr-based alloys and steam produces additional heat that compounds with residual radioactive decay heat, simultaneously producing flammable hydrogen gas as a byproduct. Therefore, any potential ATF cladding candidate should outperform Zr-based alloys during these postulated accident scenarios while maintaining the other beneficial qualities desired for nuclear cladding, including high thermal conductivity, phase stability, and sufficient neutron economy. The FeCrAl alloys represent one ATF candidate that could be deployed in existing boiling water reactors (BWRs) as a drop-in replacement for Zr-based alloys. Coupled with a highly adherent and stable aluminum oxide layer that prevents cladding deterioration in high-temperature steam, the accident tolerance of the FeCrAl alloy system has made it competitive with nearer-term ATF solutions such as Cr-coated Zr alloys. However, there is a need to assess the potential gains afforded by the FeCrAl ATF concept over the existing zirconium-based materials employed today. The unirradiated FeCrAl alloys have been tested extensively with the Severe Accident Test Station (SATS) at the Oak Ridge National Laboratory (ORNL) [3]. A parametric study varying the temperature FeCrAl oxidation kinetics was conducted by Robb et al for a BWR plant using unirradiated FeCrAl fuel cladding [4]. In this work, a steam oxidation study of irradiated FeCrAl fueled cladding was performed under the same test conditions in the SATS as Robb et al used [4].

Irradiation campaigns on the first fueled irradiation experiments on ATF concepts, referred to as ATF-1, began at the Idaho National Laboratory (INL) Advanced Test Reactor (ATR) in 2014. These irradiations were intended to screen many different concepts to ensure fuel–cladding compatibility and to provide irradiated material for future testing. The irradiation included three FeCrAl-UO_2 drop-in rodlets fabricated at ORNL targeting burnup values of 10, 30, and 50 GWd/MT. Irradiation and initial post-irradiation examination (PIE) were performed for the lowest burnup capsule (ATF-18) at INL [5]. After the initial PIE was completed, the capsule was transported to ORNL's Irradiated Fuels Examination Laboratory (IFEL) hot-cell facility for additional PIE and steam oxidation tests in the SATS.

The SATS testing revealed enhanced oxidation on the inner surface of the ATR-irradiated FeCrAl specimen, which had been subjected to 1300°C for 1 min. This novel observation underscores the potential influence of irradiation, fuel–cladding interactions, or a combination of both on the high-temperature oxidation resistance of FeCrAl alloys. To discern the underlying factors contributing to the enhanced FeCrAl oxidation observed in the ATF-1 PIE, further investigations were undertaken. These investigations aimed to determine whether irradiation-induced effects, distinct from those linked to fuel interactions, might have contributed to enhanced oxidation kinetics.

The evaluation included high-temperature oxidation tests performed on short FeCrAl tubing specimens irradiated up to an exposure of 23 displacements per atom (dpa) at the High Flux Isotope Reactor (HFIR). Unlike the ATF-18 specimen, the tubing samples did not include UO_2 pellets under irradiation. Subsequent to oxidation exposure, microstructural examinations of the specimens were conducted. These examinations involved capturing cross-section images, enabling the precise measurement of the oxidation layer thickness, and facilitating a comprehensive view of the post oxidation microstructural features.

2. MATERIALS AND IRRADIATION SUMMARY

2.1 ATR Irradiation of FeCrAl-UO_2 Rodlets

ORNL fabricated three FeCrAl rodlets containing UO_2 for irradiation within ATR known as “ATF-17,” “ATF-18,” and “ATF-19.” The ATF-18 capsule contained an early variation of an FeCrAl alloy called C35MN, which is Fe-13Cr-5Al with additions of 2Mo and 1Nb [6]. The cladding was filled with UO_2 pellets and irradiated to a burnup of 10.4 GWd/MTU [7]. The outer diameter of the cladding was approximately 0.94 cm, and the inner diameter was approximately 0.83 cm. The cladding tubes used in this irradiation were created by gun drilling rather than extrusion, which is the typical fabrication method for cladding tubing. The gun drilling created a nonprototypic surface roughness on the tube inner diameter, but this difference might be inconsequential in studying the fuel–cladding interaction. Early irradiation testing results and out-of-pile testing suggested the irradiated FeCrAl variant was susceptible to microcracking during irradiation. The ATF-1 experiment was double encapsulated with a stainless steel “capsule” that surrounded the rodlet. This capsule consisted of the sealed C35MN cladding tube and fuel pellets. Because of the uncertainty around the hermeticity of the FeCrAl tube after irradiation, the outer Stainless Steel 316 encapsulation capsule of ATF-18 was punctured, and the gas between the capsule and the C35MN rodlet was sampled before the inner rodlet was retrieved. Fission gas was detected in the capsule atmosphere, and the fission gas release was determined to be 0.35%. Note the outer capsule of this irradiation experiment was hermetically sealed, and the C35MN rodlet was only exposed to the helium atmosphere inside the capsule not any water from the ATR primary coolant. This level of release is in line with expectations from the Vitanza curve for irradiated UO_2 fuel [8]. After the rodlet was removed from the capsules, visual exams and neutron radiography were performed on the rodlet, but no obvious flaws were detected [5]. Figure 1 shows the neutron radiography results for the ORNL loss-of-coolant accident (LOCA) ATF-18 rodlet, including cracking in the UO_2 pellets [3]. The cladding diameter measured after irradiation was 9.39 to 9.40 mm, as shown in Figure 1. This diameter is larger than expected from the nominal diameter noted in the drawings (9.37 mm). However, the cladding outer diameter is within the tolerance of the drawings, indicating that no irradiation-induced diameter changes likely occurred. Unfortunately, the as-built diameter was not recorded. An oversized rodlet reduces the gap between the rodlet and the capsule, thereby reducing the irradiation temperature of the cladding and the fuel in the ATF-1 irradiations.

After irradiation and nondestructive examination at INL, the ATF-18 rodlet was shipped to the ORNL hot cells. The irradiated rodlet was sectioned into several samples for high-temperature steam oxidation tests. During sectioning, it was noted that the fuel was not firmly bonded to the cladding and could be readily removed from small cladding slices. This phenomenon was expected for a drop-in style irradiation in ATR in which no external pressure drives the cladding creep-down that is normally seen in light-water reactors. To prepare for high-temperature oxidation testing, the fuel was removed from the cladding segments.

2.2 HFIR Irradiation of Unfueled Cladding Segments

The irradiation capsule design for irradiation testing of cladding tubes in HFIR is described in Petrie et al [9]. In summary, the capsule accommodates two cladding tubes that are inserted around a Mo sleeve. Two passive silicon carbide (SiC) temperature monitor (TM) devices are inserted in each sleeve and analyzed after irradiation via dilatometry to confirm capsule irradiation temperature [10]. The irradiation temperature is controlled by the gas fill in the capsule, the gas gap between the cladding tubes, and the housing inner wall. Centering thimbles located on each end of the cladding tube/sleeve assembly are held in place by wires. The thimbles maintain the assembly centered inside the capsule housing tube and ensure a constant gas gap between the cladding specimen and the housing during irradiation. The housing is directly cooled from the outside by the reactor's primary coolant. Grafoil insulator disks are placed on each end of the capsule to reduce axial heat losses.

Capsules were assembled according to the capsule design shown in Figure 2 and were used for irradiation of FeCrAl alloy cladding tube specimens. HFIR cycles typically last about 25 days, and the cladding tube irradiation campaign included capsules that targeted either 8 or 11 total cycles. After irradiation, the capsules were shipped to the Irradiated Materials Examination and Testing (IMET) hot-cell facility for disassembly. Once the capsules were disassembled, the passive SiC TMs were shipped to the Low Activation Materials Development and Analysis laboratory for analysis to confirm the irradiation temperature, and ring specimens of about 5 mm in height were cut from each cladding tube specimen for high-temperature steam oxidation testing in the SATS. Table 1 summarizes the irradiation conditions of the various FeCrAl alloy ring specimens produced from irradiated cladding tube specimens. The specimens' average irradiation temperatures were obtained from dilatometry analysis of the TMs [10], and irradiation damage was estimated using the web-based tool described in Burns et al [11]. Specimen compositions are detailed in Yamamoto et al [6].

3. RESULTS

High-temperature steam oxidation tests of the FeCrAl specimens were performed in the SATS at the IFEL. SATS consists of two modules: one for integral testing LOCA scenarios and the other with a high-temperature furnace for testing fuel segments [12-13]. The LOCA furnace has been successfully used in LOCA fragmentation tests on high-burnup fuels [14-15]. The tests of ATR- and HFIR-irradiated FeCrAl specimens presented in this work were conducted in the high-temperature furnace. The test temperature was monitored and recorded with a Type-B thermocouple in the furnace. The uniform heating zone of the furnace is approximately 75 mm. Since the maximum specimen length is less than 5 mm, we consider the temperature distribution in whole specimen is uniform.

All tests of FeCrAl specimens were conducted at the same heating rate. The specimen was first heated from room temperature to 600°C under an Ar atmosphere at a rate of 20°C/min. Then the Ar supply was shut off, steam was supplied to the test section, and the temperature was increased to 1200°C at 7.5°C/min. The sample was either held at 1200°C or was slowly heated to 1300°C at 1.82°C/min to avoid temperature overshoot. Steam was supplied to the test section by injecting water into a preheated furnace at about 200 mL/h.

3.1 Steam Oxidation Tests with Unirradiated ATF-18 Surrogates

Before the in-cell oxidation tests of the irradiated specimen, out-of-cell benchmark tests were conducted on C35MN surrogates (same alloy, heat, and fabrication procedure as the ATR-irradiated specimens) to provide baseline data for the in-cell tests. These out-of-cell tests with unirradiated C35MN surrogates parallel the thermal history of the in-cell tests with irradiated AFT-18 specimens, particularly to reveal how the FeCrAl alloy C35MN tubing would perform at temperatures of at least 1200°C.

All tests were performed at atmospheric pressure. The surrogate specimens were approximately 9.40 mm outer diameter and 12.50 mm long. The tests and the temperature at which the tests were stopped are illustrated in Figure 3. Pre- and post-oxidation test mass measurements were performed to determine the specimen weight gain.

To determine an accurate posttest specimen weight, the specimen must be free of moisture. Dryness was ensured by measuring the specimen mass several times after it was dried in air up to 4 h, or until the mass did not change. The posttest specimen weight was measured to the nearest 0.01 mg using a calibrated balance. The weight gain was determined by subtracting the pretest weight from the posttest weight and normalizing this value to the steam-exposed surface area of the specimen. The surface area of the specimen was calculated by including the inner tube surface, the outer tube surface, and both ends.

Table 2 lists the test conditions, weight gain, and measured oxide layer thicknesses from the steam oxidation tests of unirradiated FeCrAl alloy C35MN tubing specimens. Specimens melted as soon as the temperature reached 1400°C. However, the C35MN was very stable at 1300°C. Posttest images of these tests are provided in Figure 4. The oxidation pickup of the FeCrAl alloy is likely characterized by a parabolic rate law. For the oxidation tests at 1300°C, the heating and cooling durations were the same. Therefore, the oxidation at the hold temperature can be considered an isothermal process, and the oxidation rate can be considered a constant for the multi-oxidation tests at a target temperature [16-17].

Figure 5 shows parabolic oxidation curves of the unirradiated C35MN specimens oxidized at 1300°C. The test data points vs. the isothermal oxidation time are in good agreement with a linear fit to the experimental data, indicating good control of isothermal oxidation temperature. For isothermal oxidation at a target temperature of 1300°C, the weight-gain coefficient was determined to be 3.8×10^{-3} $(mg/cm^2)/s^{1/2}$ by the slope of the fits in Figure 5. This value is about two orders of magnitude less than the coefficient of Zr alloys.

The microstructure of the steam-oxidized specimens was examined. Metallographic mounts were prepared and examined using optical microscopy to image the cross-sectional metal layers, the oxide layers, and their interfaces. Figures 6–7 show the outer diameter and inner diameter surface images, respectively, for the ATF-18 surrogate specimens subjected to steam oxidation at 1300°C. The thickness of the outer- and inner-diameter oxide layers were uniform and well defined, so the oxide layer thickness was measured at azimuthal locations of the cross section of the metallographic mounts. The measured oxide layer thicknesses are given in Table 2.

3.2 Steam Oxidation Tests with ATR-Irradiated ATF-18 Specimens

Pre-oxidation test characterization was performed on the ATF-18 rodlet to determine the fuel, fuel–cladding bond, and cladding behavior. Figure 8a shows a low-magnification image of the fuel morphology. The fuel partially fell out during sample preparation. The fuel–cladding bond was not observed, which is unsurprising for a low-burnup rod such as the ATF-18 and for a double-encapsulated drop-in style irradiation as stated earlier. Figure 8b shows a higher-magnification image showing a gap between the cladding and fuel.

High-temperature steam oxidation tests of the irradiated ATF-18 specimens were performed with the in-cell SATS. To ensure fuel removal, the fuel was dissolved in HNO_3 at room temperature from segments of the cladding before high-temperature oxidation testing. The measured outer diameter of the ATF-18 rodlet was approximately 9.40 mm. The sample length for the high-temperature oxidation tests was between 4.5 and 7.0 mm.

All in-cell tests of irradiated ATF-18 specimens were conducted under the same temperature heating rates as the out-of-cell tests for unirradiated surrogate specimens. The specimen was first heated from room temperature to 600°C under an Ar atmosphere at a rate of 20°C/min. Then the Ar supply was shut off, steam was supplied to the test section, and the temperature was increased to 1200°C at 7.5°C/min. The sample was either held at 1200°C or slowly heated to 1300°C at 1.82°C/min. The tests and temperatures at which the in-cell tests were stopped are illustrated in Figure 9.

Although unirradiated specimens performed very well at 1300°C, the ATR-irradiated specimens started enhanced oxidation as soon as the temperature reached 1300°C. However, the ATF-18 specimen was very stable at 1200°C. Furthermore, the oxygen pickup at 1200°C was extremely low: under the limit of the scale for weight-gain measurements. Posttest images of these tests at 1200° and 1300°C are provided in Figures 10 and 11. Table 3 lists the test conditions and results of the steam oxidation tests of irradiated ATF-18 defueled tubing specimens.

The microstructures of the ATF-18 oxidation specimens were examined using optical microscopy. Figure 12 shows low-magnification images for ATF-18 specimens after the high-temperature oxidation in the SATS. Micrographs at eight azimuthal locations (every 45°) of the cross sections of the metallographic mounts were taken at higher magnification, as shown schematically in Figure 13.

Enhanced oxidation was observed on the inner surface at several areas of the ATF-18F1 (Figure 12d and Figure 13), which was oxidized at 1300°C for 1 min. This phenomenon was not observed for unirradiated ATF-18 surrogate specimens oxidized in steam at 1300°C for up to 240 min. Enhanced oxidation was not observed in the irradiated specimens oxidized at 1200°C. However, higher-magnification images revealed some cracks in the specimens oxidized at 1200°C. It is not clear when these cracks occurred. They were likely caused by handling and sample preparation during PIE, but they could have occurred during irradiation or during tube fabrication. As noted in Section 2, fission gas was present in the irradiation capsule containing the rodlet after irradiation, so this crack may have opened during irradiation, possibly as a fabrication defect.

3.3 Steam Oxidation Tests with HFIR-Irradiated Specimens without UO_2

For comparison, HFIR-irradiated FeCrAl specimens underwent steam oxidation tests using the in-cell SATS high-temperature furnace. The specimens were cladding only, without fuels. Nominal outer diameter was 9.50 mm, and nominal wall thickness was 0.375 mm. Table 4 is the test matrix for in-cell SATS tests of HFIR-irradiated FeCrAl specimens. All in-cell steam oxidation tests of HFIR-irradiated specimens occurred under the same test conditions as for the ATR-irradiated specimens. The sample was slowly heated to 1300°C (see Figure 14). The tests and temperatures at which the in-cell tests were stopped are illustrated in Figure 14.

Although the ATR-irradiated ATF-18 specimen started enhanced oxidation as soon as the temperature reached 1300°C, the HFIR-irradiated FeCrAl specimens were stable at 1300°C. Posttest images of these specimens at 1300°C for 1, 90, and 240 min are provided in Figure 15a–c. No enhanced oxidation was observed for these specimens. After the oxidation tests, the specimens were examined using optical microscopy to view the cross-sectional metal layers, the oxide layers, and their interfaces. Figures 16–18 show micrographs for the HFIR-irradiated FeCrAl specimens oxidized for 1, 90, and 240 min at 1300°C, respectively. Table 5 lists the oxide layer thicknesses from the steam oxidation tests of the HFIR-irradiated FeCrAl specimens. To compare the oxidation between the irradiated and unirradiated specimens, the measured oxide layer thicknesses vs. time are plotted in Figure 19 for the irradiated and unirradiated FeCrAl specimens that were evaluated under the same oxidation conditions. The oxide layers of the HFIR-irradiated FeCrAl tubing specimens are slightly thinner than unirradiated FeCrAl, but the difference is not significant and is within the measurement uncertainty from optical imaging. The alloy C36M (79Fe-13Cr-6Al-2Mo) oxidation rates are the same after being irradiated in HFIR for 8 and 11 cycles.

4. Discussion

These experiments demonstrate that something unique occurs when FeCrAl is near UO_2 during neutron irradiation that is not related to pure neutron irradiation. The oxidation behavior of this test FeCrAl alloy in the unirradiated state follows the expected behavior for FeCrAl alloys in which oxidation is minimal at 1300°C. Similarly, the same FeCrAl alloy was neutron irradiated in HFIR and showed no change in oxidation behavior between the unirradiated state and irradiated state. This result demonstrates that neutron irradiation alone does not affect the oxidation behavior of FeCrAl alloys. The outer diameter of the ATF-18 samples also demonstrates that oxidation proceeds normally for the metal far away from the fuel–cladding interface. Even in the ATF-18 samples, the oxidation resistance behavior of the FeCrAl samples is far superior to the behavior of Zr alloys at 1200°C.

In the event of cladding breach, the phenomenon observed in this testing may be important for understanding severe accidents in FeCrAl-UO_2 fueled reactors. To understand the observed enhanced oxidation, scanning electron microscopy (SEM) with energy dispersive spectroscopy (EDS) was performed on three samples from the ATF-18 irradiation. This examination included an as-irradiated sample (ATF-18B), the sample tested at 1200°C for 90 min (ATF-18G2), and the sample tested at 1300°C for 1 min (ATF-18F1). Figure 20 shows these samples. Just as in the optical microscopy (Figure 8), no evidence of interaction in the as-irradiated sample between the fuel and the FeCrAl was observed via SEM. The composition of the FeCrAl appears constant across the sample, and no fission products were observed interacting with the FeCrAl at the limits of detection for EDS. Furthermore, no signs of oxidation or secondary phases were observed at the fuel–cladding interface, as observed in other FeCrAl-UO_2 irradiations [18]. An approximately 2.5 µm alumina layer formed on the inner and outer surface of the ATF-18 sample oxidized at 1200°C for 90 min, as expected from oxidation testing of the unirradiated and HFIR-irradiated samples. This layer appeared to be well adhered on both sides of the sample and was relatively uniform. The ATF-18 sample oxidized at 1300°C for 1 min exhibited many different behaviors. The outer diameter of the sample had a thin, approximately 1 µm alumina layer that is similar to the alumina layer formed by the 1200°C samples and those formed by the unirradiated and HFIR-irradiated samples. In many locations on the inner diameter, a similar approximately 1 µm alumina layer was present (Figure 20). However, certain locations exhibited areas of high porosity near the alumina layer. In these areas, the alumina layer appears to have begun to detach from the FeCrAl substrate. This separation led to areas of excessive oxidation in the sample. An example of this oxidation is shown in Figure 21. Examination by EDS of the interaction areas revealed that the oxide that grew beyond the original sample surface was primarily iron oxide without any Al or Cr. The oxide in the prior sample surface area was also Al depleted, but it did contain Cr mixed with the Fe. The Al appears at the interface between the oxide and the metal, but it does not appear to form a coherent protective layer. This phenomenon is illustrated by EDS maps in Figure 21.

The lack of a protective alumina scale at certain locations along the inner cladding surface may be explained from recent lower-length scale investigations of FeCrAl-UO_2 diffusion couples also irradiated as part of the ATF-1 irradiation experiment [19]. In their work, Haozheng et al. found that a nanoscale amorphous layer, rich in Al and U, formed at the FeCrAl-UO_2 interface. This amorphous is likely from pure P/C interaction because the neutron irradiation temperature is around 300°C. Because previous results indicate that an optimal combination of both Al and Cr is necessary to ensure a passivating oxide layer on the surface of FeCrAl during oxidation [20], one potential explanation for the deterioration of oxidation performance is the local depletion of Al from the matrix to form the (U, Al)-rich layer, thereby reducing available Al in the matrix to prevent oxidation. Unfortunately, any confirmatory transmission electron microscopy investigations on the present samples are impossible because the material was consumed by the rapid oxidation at 1300°C. Furthermore, the SEM–EDS analyses in this work suggest that any local depletions in Al are on a spatial resolution unresolvable in the length scales investigated in this work.

This examination further illustrates the excessive oxidation experienced by the FeCrAl samples irradiated in contact with UO_2 when exposed to high-temperature steam, but it does not fully explain why the alumina layer lost its cohesion, leading to excessive oxidation. These studies suggest the absence of any large-scale change in the chemical composition of the FeCrAl or large-scale chemical interaction between the UO_2 and FeCrAl at the fuel–cladding interface. However, the results from oxidation of the HFIR-irradiated specimens suggest that the change in oxidation behavior is not caused purely by neutron-induced radiation damage or neutron-induced transmutation in the FeCrAl. The outer-diameter oxidation of the ATF-18 sample further confirms this behavior. Consequently, additional work is ongoing on available FeCrAl-UO_2 segments to capture potential U or other fission product interactions near the fuel–cladding interface.

5. CONCLUSIONS

The FeCrAl-UO_2 test capsules were fabricated at ORNL and irradiated at ATR. After irradiation, samples were sectioned from the irradiated rod ATF-18 for oxidation kinetics study to assess the candidate cladding high-temperature oxidation performance. The results indicate the ATR-irradiated FeCrAl C35MN alloy provided good thermal stability up to 1200°C. However, although the unirradiated C35MN surrogate specimens were very stable at 1300°C for 240 min, the ATF-18 specimens started enhanced oxidation as soon as the temperature reached 1300°C. The SATS testing revealed enhanced oxidation on the inner surface of the ATR-irradiated FeCrAl specimen, which had been subjected to 1300°C for 1 min. This novel observation underscores the potential influence of irradiation, fuel–cladding interactions, or a combination of both on the high-temperature oxidation resistance of FeCrAl alloys. To discern the underlying factors contributing to the enhanced FeCrAl oxidation observed in the ATF-1 PIE, further investigations were undertaken. These investigations aimed to determine whether irradiation-induced effects, distinct from those linked to fuel interactions, might have contributed to enhanced oxidation kinetics.

The evaluation included high-temperature oxidation tests performed on short FeCrAl tubing specimens irradiated up to an exposure of 23 dpa at HFIR. Unlike the ATF-18 specimen, the tubing samples did not include UO_2 pellets under irradiation. The results indicate that the HFIR-irradiated FeCrAl provided good thermal stability at 1300°C. No enhanced oxidation was observed for the HFIR-irradiated specimens oxidized at 1300°C for up to 240 min. Therefore, the enhanced oxidation of the ATF-18 specimen likely results from fuel–cladding interaction at 1300°C. SEM examination of the ATF-18 samples was inconclusive regarding the discovery of a clear mechanism for the excessive oxidation, but it did clarify that the nature of the excessive oxidation is limited to the inner diameter of the cladding that is in contact with UO_2 during irradiation. Further study of irradiated FeCrAl alloys with UO_2 should be undertaken to elucidate the mechanism of enhanced oxidation at temperatures above 1300°C.

ACKNOWLEDGMENTS

This research was sponsored by the Advanced Fuels Campaign Program of the US Department of Energy Office of Nuclear Energy. The article was authored by UT-Battelle under Contract No. DE-AC05-00OR22725 with the US Department of Energy. The authors would like to thank Tyson Jordan and Zach Burns for their hot-cell expertise, preparing the specimens, and providing sample images.

References

[1] S.J. Zinkle, K.A. Terrani, J.C. Gehin,; L.J. Ott, L.L. Snead, Accident tolerant fuels for LWRs: A perspective. J. Nucl. Mater. 2014, 448, 374–379. https://doi.org/10.1016/j.jnucmat.2013.12.005.

[2] M. Kurata, Research and Development Methodology for Practical Use of Accident Tolerant Fuel in Light Water Reactors. Nucl. Eng. Technol. 2016, 48, 26–32. https://doi.org/10.1016/j.net.2015.12.004.

[3] B. Pint and J.W. McMurray, Steam Oxidation Testing in the Severe Accident Test Station, ORNL/LTR-2016/425. August 2016.

[4] K. Robb, M. Howell, and L. Ott, Parametric and Experimentally Informed BWR Severe Accident Analysis Using FeCrAl, ORNL/SPR-2017/373, August 2017.

[5] Jason M. Harp, Fabiola Cappia, and Luca Capriotti, *Postirradiation Examination of the ATF-1 Experiments—2018 Status*, INL/EXT-18-51497, September 2018.

[6] Y. Yamamoto, B. A. Pint, K. A. Terrani, K. G. Field, Y. Yang and L.L. Snead, "Development and Property Evaluation of Nuclear Grade Wrought FeCrAl Fuel Cladding for Light Water Reactors," *Journal of Nuclear Materials*, 467 (2015) 703–716.

[7] C. J. Murdock, B. J. Curnutt, C. Hale, *Accident Tolerant Fuels Series 1 (ATF-1) Irradiation Testing FY 2018 Status Report*, INL/EXT-18-51584, September 2018.

[8] C. Vitanza, E. Kolstad, U. Graziani, Fission gas release from UO2 pellet fuel at high burn-up, in: Proc. Am. Nucl. Soc. Top. Meet. Light Water React. Fuel Perform., 1979.

[9] C.M. Petrie, R.H. Howard, K.R. Smith, C.R. Daily, Analysis and Experimental Qualification of an Irradiation Capsule Design for Testing Pressurized Water Reactor Fuel Cladding in the High Flux Isotope Reactor, ORNL/TM-2017/67, Oak Ridge National Laboratory, September 2017.

[10] K.G. Field, J.L. McDuffee, J.W. Geringer, C.M. Petrie, Y. Katoh, "Evaluation of the Continuous Dilatometer Method of Silicon Carbide Thermometry for Passive Irradiation Temperature Determination," *Nuclear Inst. and Methods in Physics Research B* 445 (2019): 46–56.

[11] J. Burns, K. Terrani, "A Web-based Application for Standardization of Radiation Damage Calculations," Transactions of the American Nuclear Society, Vol. 119, November 2018.

[12] M. Snead, Y. Yan, M. Howell, J. Keiser, and K. Terrani, *Severe Accident Test Station Design Document*, ORNL/TM-2015/556, Oak Ridge National Laboratory, September 2015.

[13] K. Linton, Y. Yan, Z. Burns, and K. Terrani, *Hot Cell Installation and Demonstration of the Severe Accident Test Station*, ORNL/SPR-2017/434, Oak Ridge National Laboratory, August 2017.

[14] Yong Yan, Zach Burns, Tyler Smith, Kory D. Linton, Ken Yueh (EPRI), and Kurt A. Terrani, *LOCA Fragmentation Test with High Burnup HBR Fuel Rod*, ORNL/TM-2019/1239, July 2019.

[15] Nathan Capps, Yong Yan, Alicia Raftery, Zachary Burns, Tyler Smith, Kurt Terrani, Ken Yueh, Michelle Bales, and ,Kory Linton, "Integral LOCA Fragmentation Test on High-Burnup Fuel," *Nuclear Engineering and Design* 367 (2020) 110811.

[16] Yong Yan, Benton E. Garrison, Mike Howell, and Gary L. Bell, "High-Temperature Oxidation Kinetics of Sponge-Based E110 Cladding Alloy," Journal of Nuclear Materials 496 (2017) 343 - 352.

[17] Yong Yan, Benton E. Garrison, Andy Nelson, and Dan Lutz, "Correlations of the Steam Oxidation Rate Constant of BWR Alloy Zircaloy-2 at 800-1400°C," Oxidation of Metals (2022) 97:227–239.

[18] F. Cappia, Post-irradiation Examinations of Accident Tolerant Fuel Candidates with Iron-alloy Cladding, Idaho Natl. Lab. Rep. (2019) INL/EXT-19-56583. https://www.osti.gov/biblio/1605999.

[19] H.J. Qu, M. Higgins, H. Abouelella, F. Cappia, J. Burns, L. He, C. Massey, J. Harp, K.G. Field, R. Howard, R.V. Umretiya, A.K. Hoffman, J.P. Wharry, R.B. Rebak, FeCrAl fuel/clad chemical interaction in light water reactor environments, Journal of Nuclear Materials 587 (2023).

[20] B.A. Pint, K.A. Terrani, Y. Yamamoto, L.L. Snead, Material selection for accident tolerant fuel cladding, Metallurgical and Materials Transactions E 2(3) (2015) 190-196.

Tables

Table 1. Summary of cladding tube irradiation conditions at HFIR

FeCrAl alloy	Compositions	Ring specimen ID	Number of HFIR cycles	Specimen average irradiation temperature (°C)	Irradiation damage (dpa)	Specimen OD (mm)	Specimen wall thickness (mm)
B126Y	82Fe-12Cr-6Al	B126Y-3-C	8	355 ± 23	16	9.510	0.375
		B126Y-4-C	11	305 ± 3	23	9.511	0.375
B136Y	81Fe-13Cr-6Al	B136Y-4-C	11	335 ± 1	23	9.526	0.368
C06M	82Fe-10Cr-6Al-2Mo	C06M-02-A	11	311 ± 5	23	9.527	0.369
C36M3	79Fe-13Cr-6Al-2Mo	C36M3-3-C	8	338 ± 11	16	9.536	0.383
		C36M3-1-C	11	334 ± 14	23	9.568	0.389

Table 2. Test conditions and weight gain for unirradiated ATF-18 surrogate C35MN tubing specimen oxidized in steam.

Test ID	Max. temperature (°C)	Time at max. temperature (min)	Measured weight gain (mg/cm^2)	Measured OD oxide (μm)	Measured ID oxide (μm)	Sample surface
1	1400 ± 7	1	N/A	N/A	N/A	Melted
2	1300 ± 7	1	0.336	2.1	2.0	Lustrous black
3	1300 ± 7	90	0.586	3.7	3.5	Lustrous black
4	1300 ± 7	240	0.762	5.4	5.0	Lustrous black

Table 3. Test conditions and results for in-cell SATS tests of ATR-irradiated ATF-18 steam specimens.

Test ID	Max. temperature (°C)	Time at max. temperature (min)	Calculated equivalent cladding reacted for Zry-4* (%)	Sample surface
H2	1200 ± 6	1	16	Lustrous black
G1	1200 ± 6	15	35	Lustrous black
G2	1200 ± 6	90	79	Lustrous black
F1	1300 ± 7	1	–	Partially melted
F2	1300 ± 7	15	–	Melted
E	1300 ± 7	90	–	Melted

*: see Ref. 16.

Table 4. Test matrix for in-cell SATS tests of HFIR-irradiated FeCrAl specimens.

FeCrAl alloy	Sample ID	DPA	Irr temp	1 min	90 min	240 min
B126Y (82Fe-12Cr-6Al)	B126Y-3-C	16	355 ± 23	✓		
	B126Y-4-C	23	305 ± 3	✓	✓	
B136Y (81Fe-13Cr-6Al)	B136Y-4-C	23	335 ± 1	✓	✓	
C06M (82Fe-10Cr-6Al-2Mo)	C06M-02-A	23	311 ± 5	✓	✓	
C36M (79Fe-13Cr-6Al-2Mo)	C36M3-3-C	16	338 ± 11	✓	✓	✓
	C36M3-1-C	23	334 ± 14		✓	✓

Table 5. Measured oxide layer thicknesses of post-oxidation HFIR irradiated FeCrAl specimens.

Sample ID	**Composition**	**Test Time at 1300°C (min)**	**OD oxide (μm)**	**ID oxide (μm)**	**Sample conditions**
B126Y-4-C	82Fe-12Cr-6Al	1	1.8	2.1	As-irradiated
C36M3-1-C	79Fe-13Cr-6Al-2Mo	90	2.8	2.9	As-irradiated
C36M3-1D-2	79Fe-13Cr-6Al-2Mo	90	3.2	3.5	As-irradiated
C36M3-3D-2	79Fe-13Cr-6Al-2Mo	90	3.2	3.6	As-irradiated
C36M3-1D-1	79Fe-13Cr-6Al-2Mo	240	4.0	4.4	As-irradiated
C36M3-3D-1	79Fe-13Cr-6Al-2Mo	240	4.2	4.6	As-irradiated

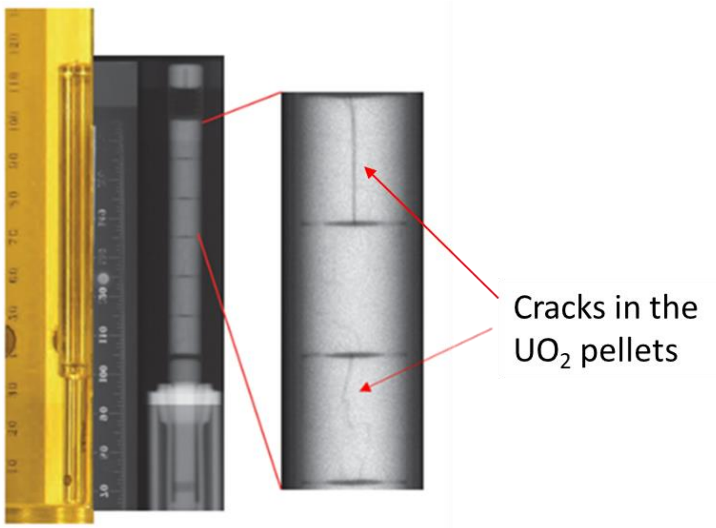

Figure 1. Visual examination and neutron radiography of the ORNL LOCA FCA-L3 rodlet. A neutron radiography detail shows cracking in the UO_2 pellets. [1].

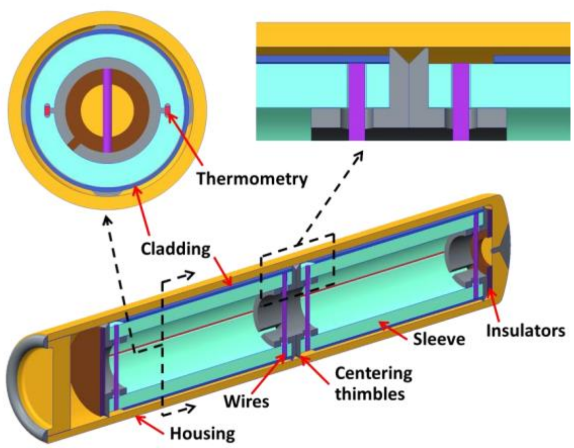

Figure 2. Section view of the irradiation capsule design for HFIR irradiation of cladding tube specimens.

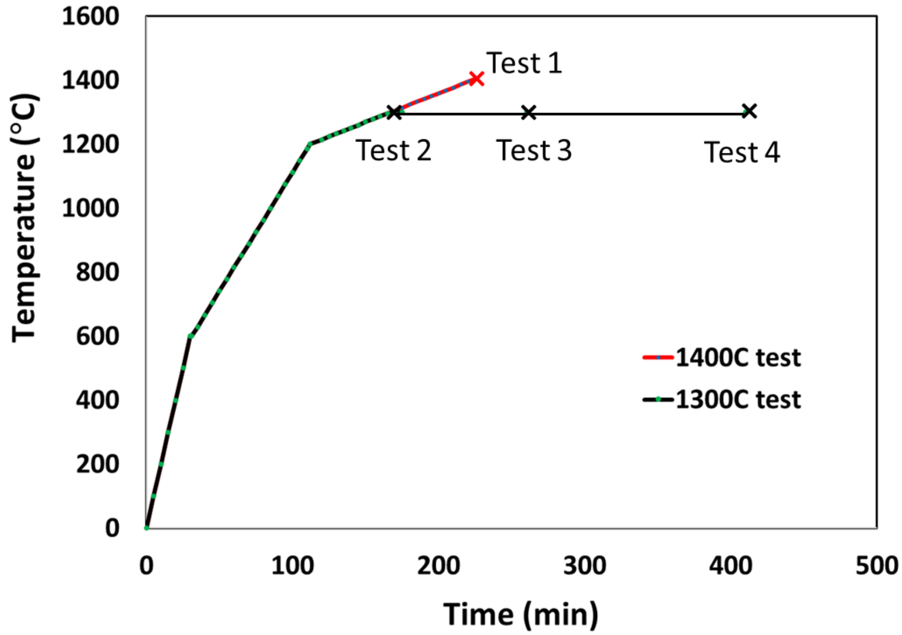

Figure 3. Heating segment illustration for out-of-cell high-temperature steam oxidation tests (see Table 2 for details).

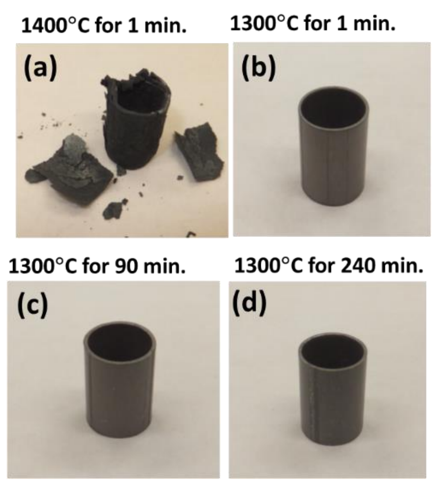

Figure 4. Posttest images of high-temperature steam-oxidized FeCrAl alloy C35MN tubing specimens.

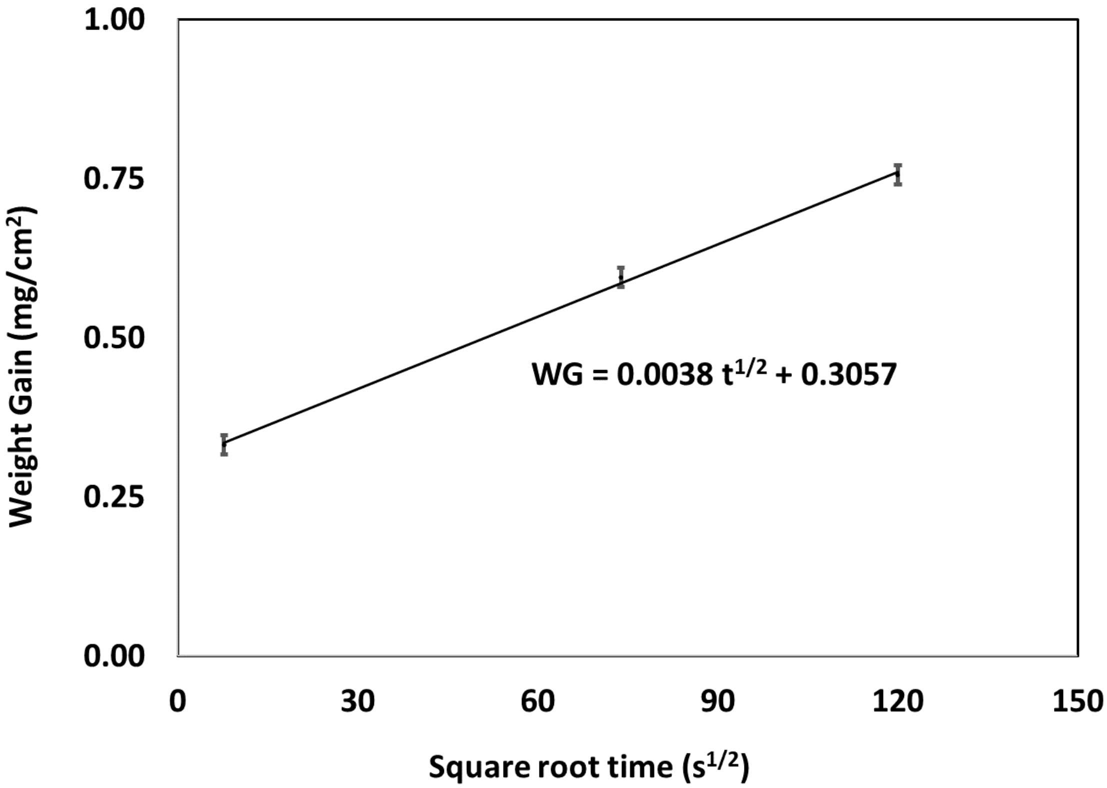

Figure 5. Steam oxidation parabolic curve of unirradiated FeCrAl C35MN at 1300°C. The estimated uncertainty of the weight gain is approximately 4%.

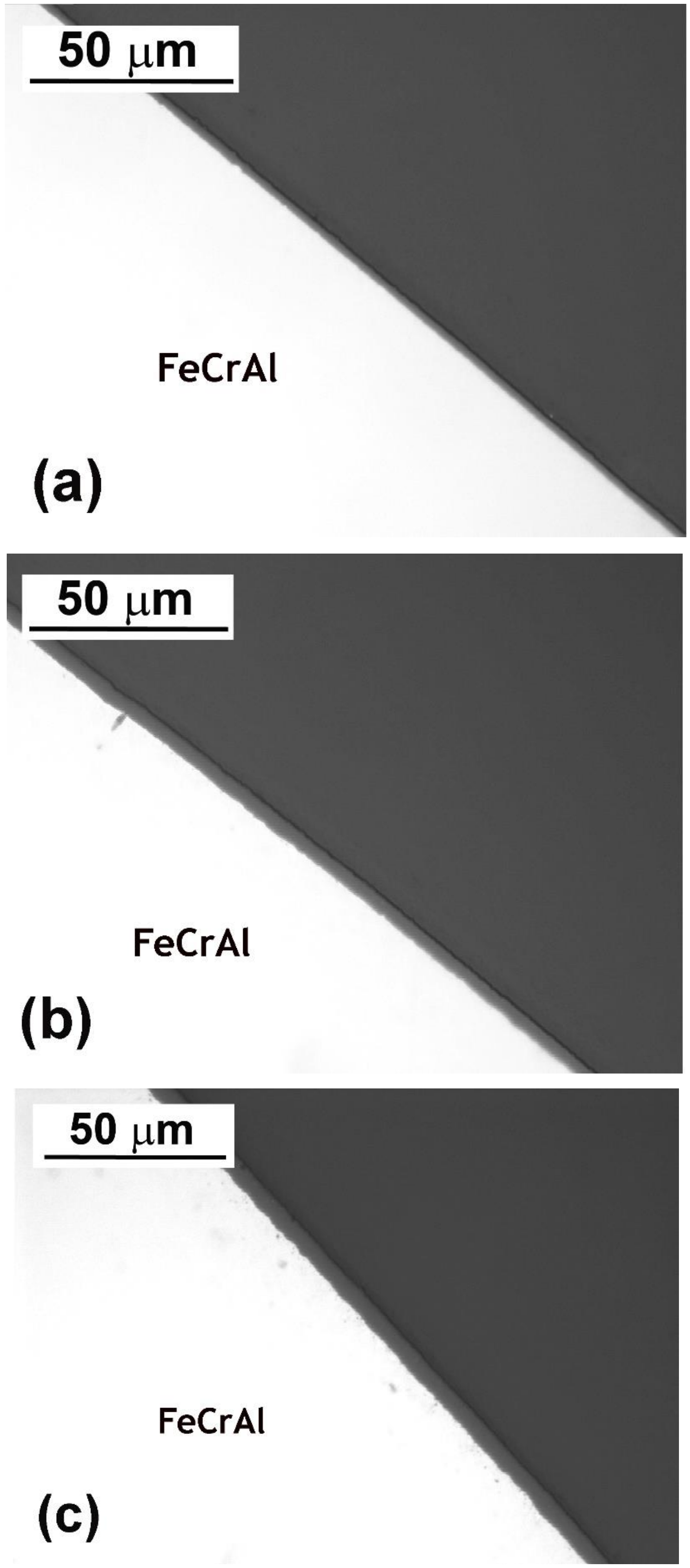

Figure 6. Micrographs of the outer-diameter surfaces of the unirradiated C35MN oxidized in steam at 1300°C for 1, 90, and 120 min.

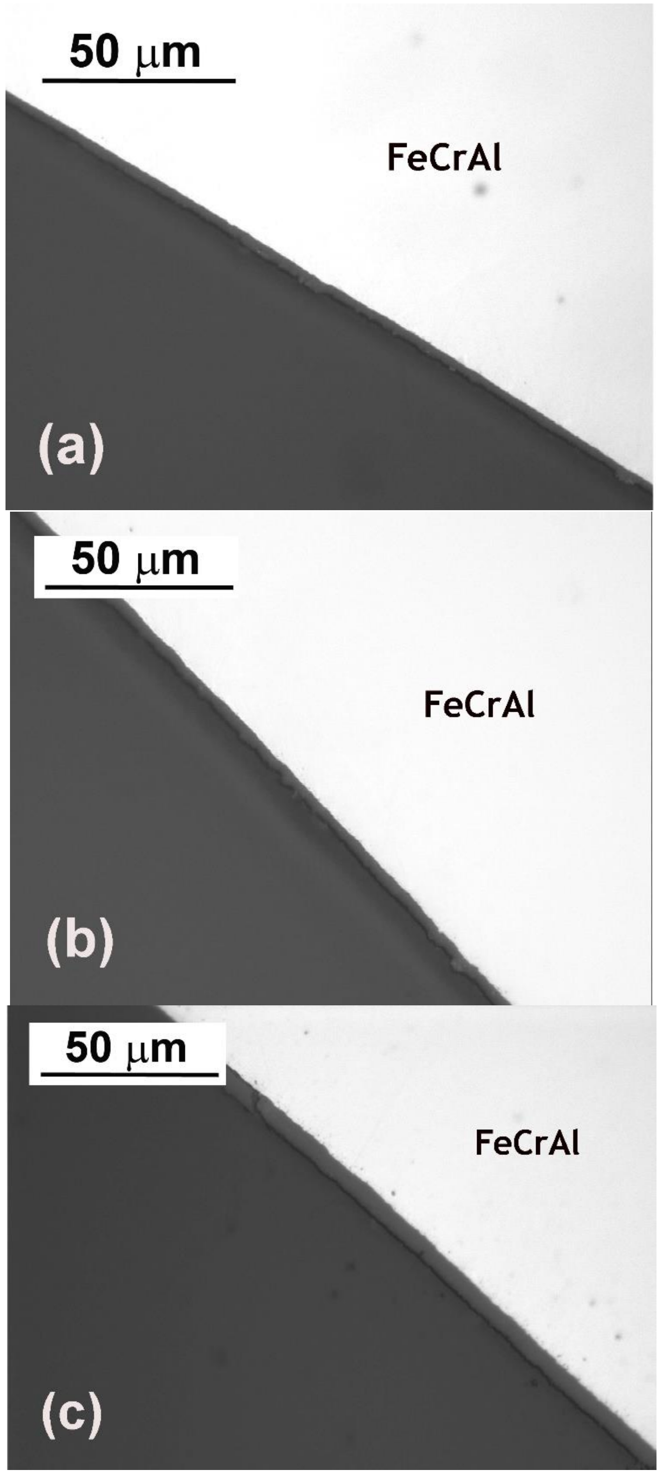

Figure 7. Micrographs of the inner-diameter surfaces of the unirradiated C35MN oxidized in steam at 1300°C for 1, 90, and 240 min.

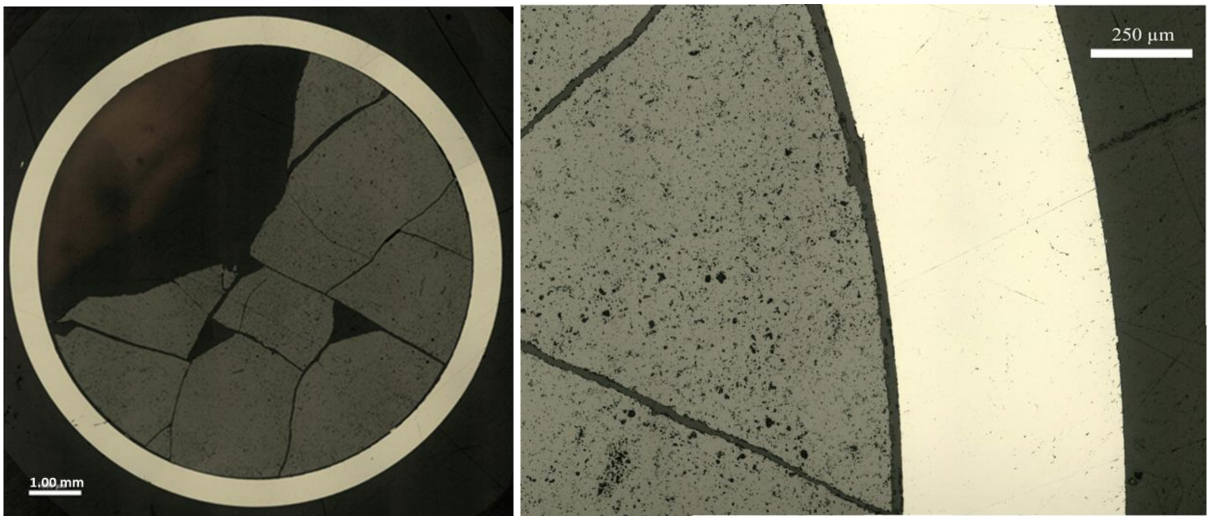

(a) (b)

Figure 8. (a) Fuel morphology for the ATF-18 rodlet, (b) high-magnification image showing a gap between the fuel and cladding.

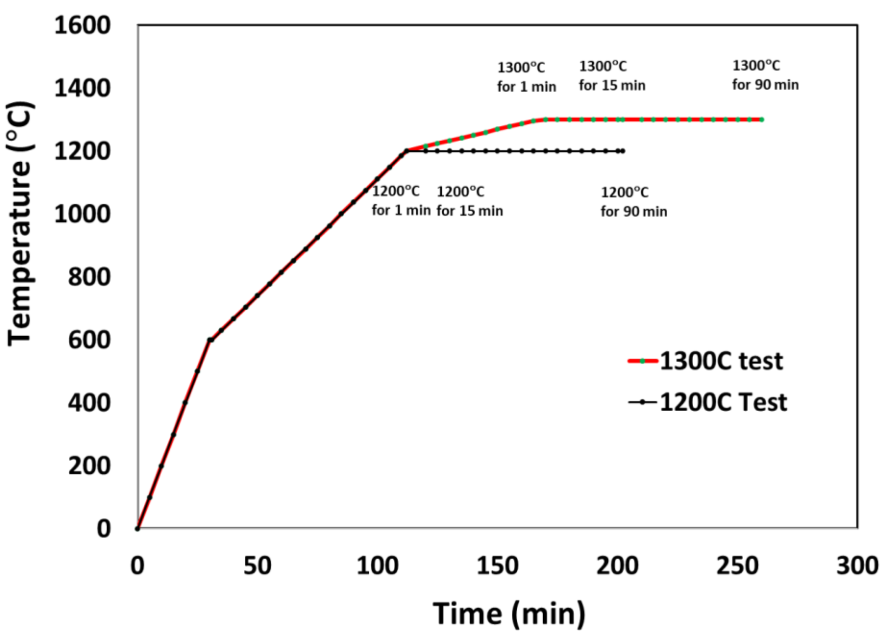

Figure 9. Heating segment illustration for in-cell high-temperature steam oxidation tests with the ATF rodlet.

Figure 10. Posttest images of irradiated ATF-18 specimens oxidized at 1200°C. The purple-blue strips are artificial effects from the camera in hot cell.

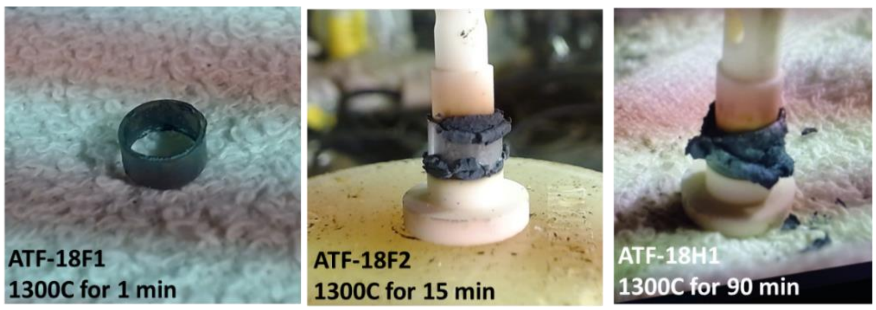

Figure 11. Posttest images of irradiated ATF-18 specimens oxidized at 1300°C. The purple-blue strips are artificial effects from the camera in hot cell.

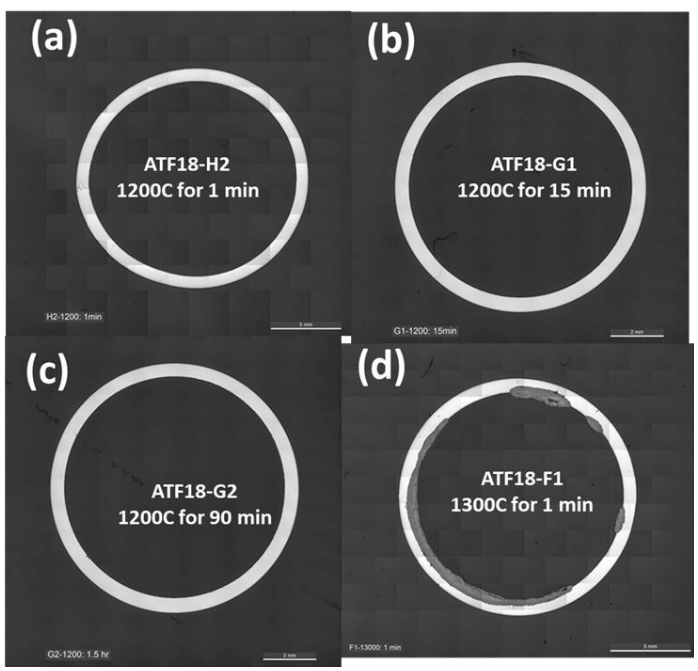

Figure 12. Low-magnification images of the irradiated ATF-18 specimens after the high-temperature oxidation in the SATS.

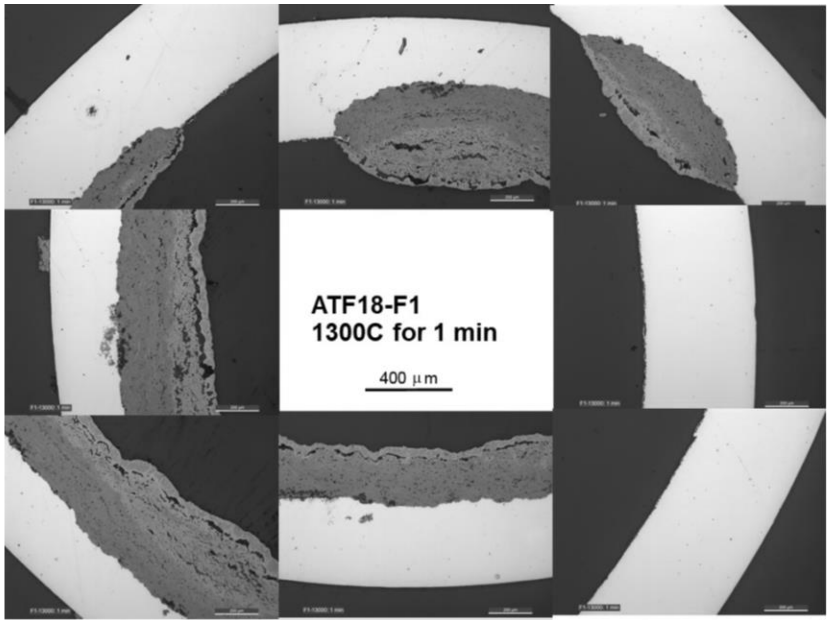

Figure 13. Images at eight locations around the circumference of ATF-18F1 specimen oxidized at 1300°C for 1 min. Local enhanced oxidation was observed on the inner surface of ATF-18F1 at several areas.

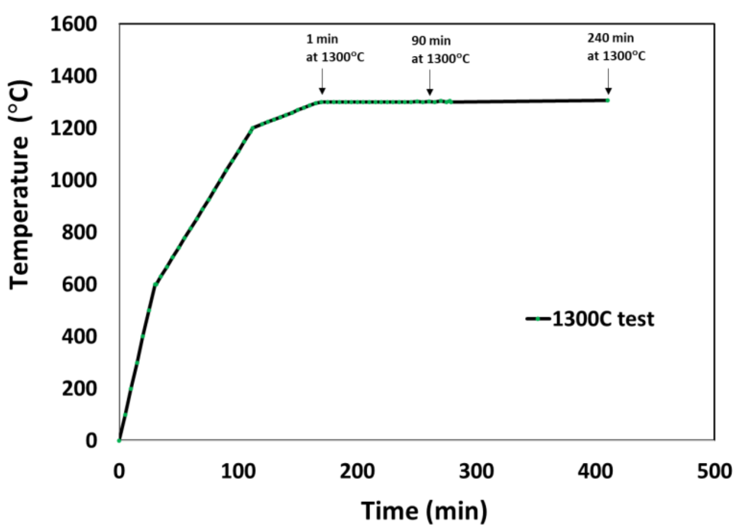

Figure 14. Heating segment illustration for in-cell high-temperature steam oxidation tests.

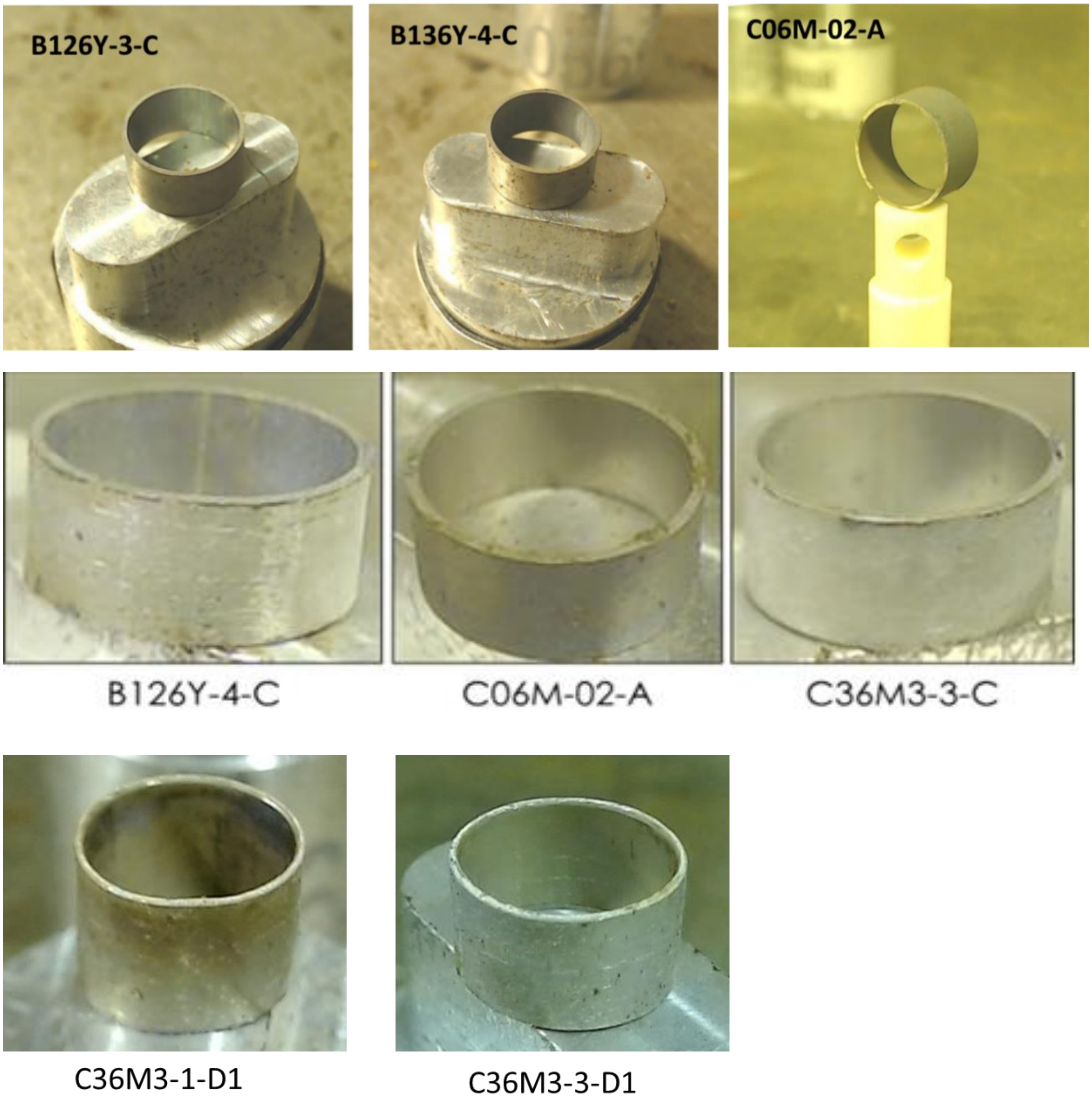

Figure 15. Post-test images of HFIR-irradiated FeCrAl specimens oxidized at 1300°C for (top row) 1 min, (middle row) 90 min, and (bottom row) 240 min.

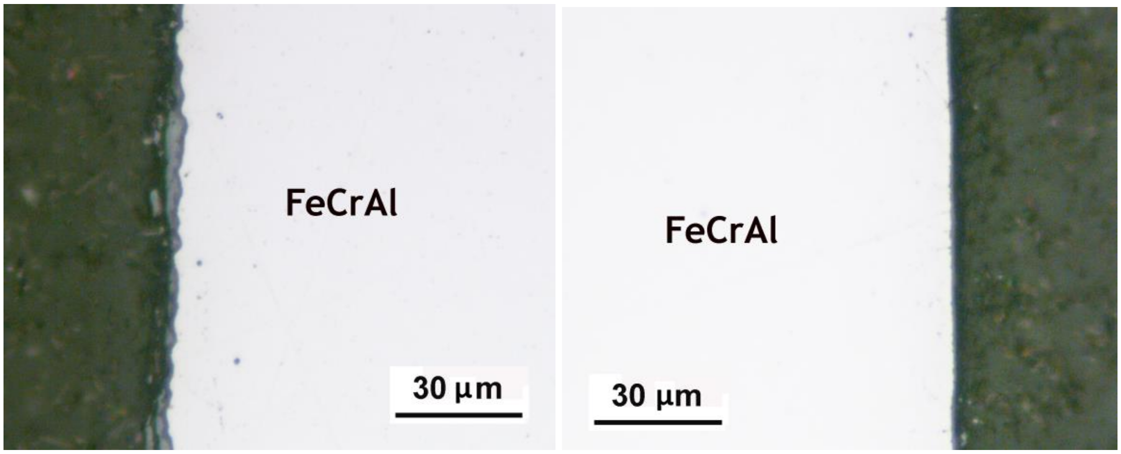

Figure 16. Micrographs of the HFIR-irradiated FeCrAl specimen B126-3 (left) inner and (right) outer surfaces after high-temperature oxidation testing at 1300°C for 1 min.

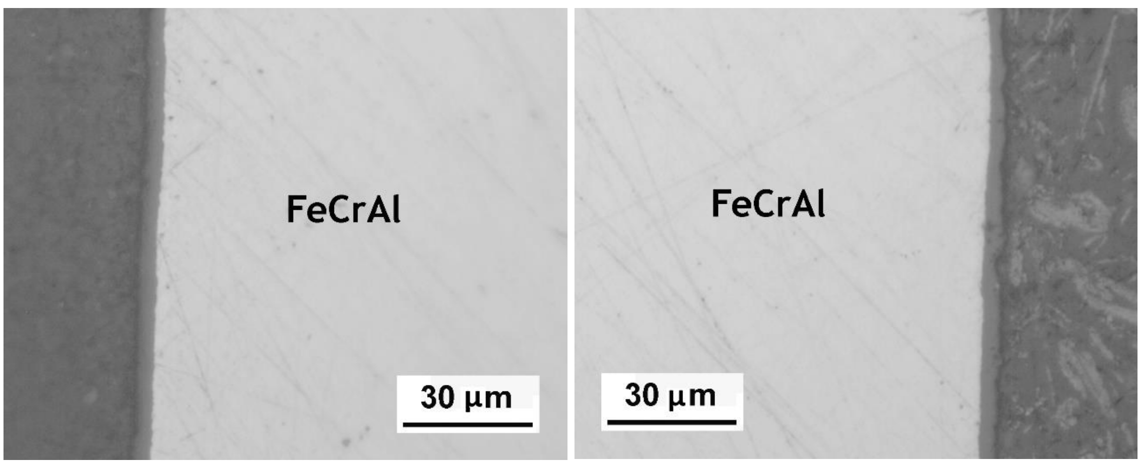

Figure 17. Micrographs of the HFIR irradiated FeCrAl specimen C36M-3-D (left) inner and (right) outer surfaces after high-temperature oxidation testing at 1300°C for 90 min.

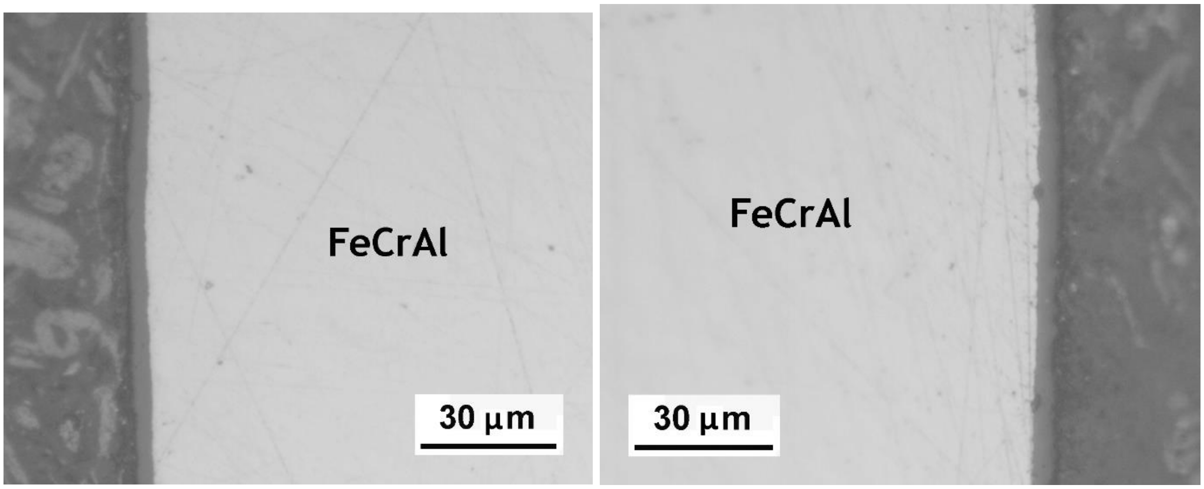

Figure 18. Micrographs of the HFIR irradiated FeCrAl specimen C36M-3-D (left) inner and (right) outer surfaces after high-temperature oxidation testing at 1300°C for 240 min.

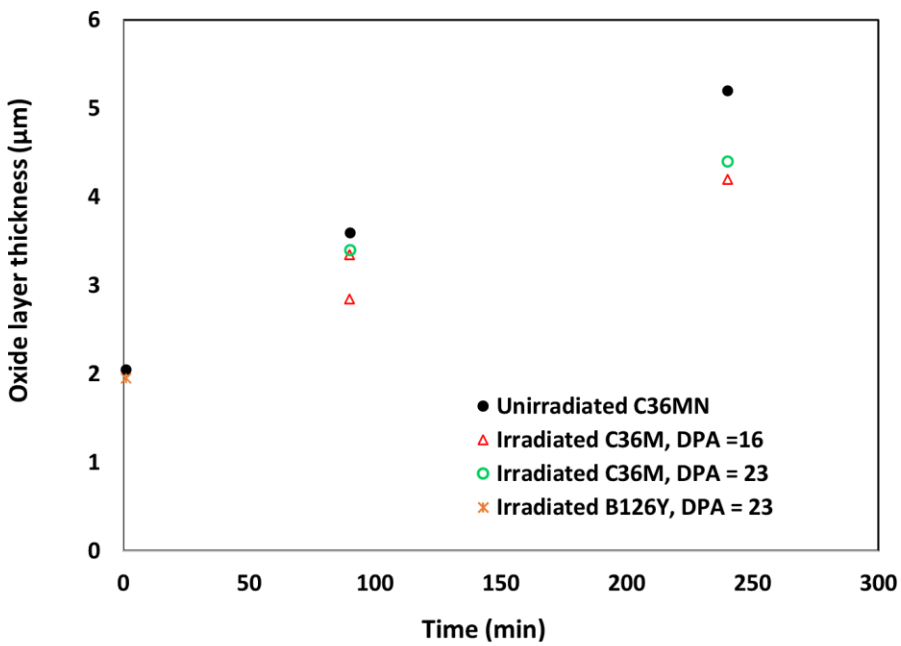

Figure 19. Oxide layer thicknesses plotted vs. time for the irradiated and unirradiated FeCrAl specimens tested in steam at 1300°C.

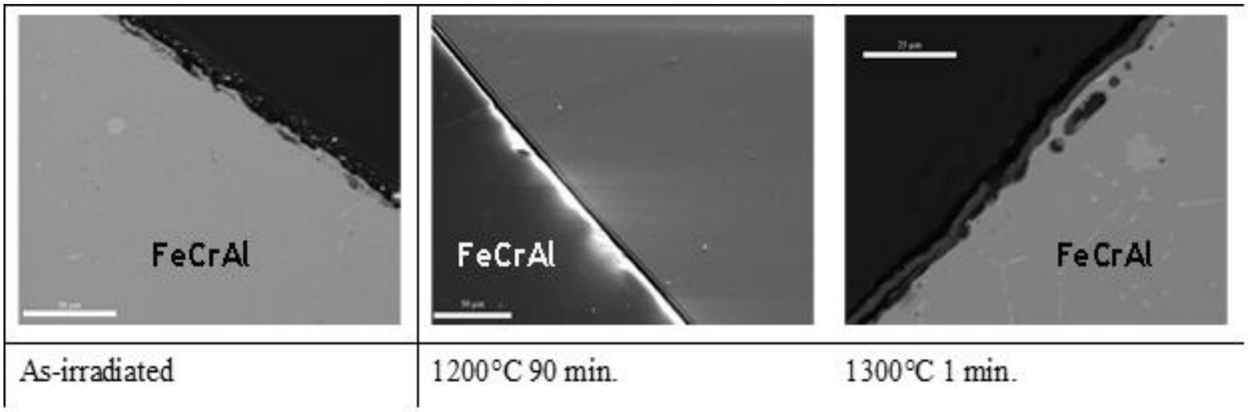

Figure 20. High-magnification backscatter electron images of the inner surface of as-irradiated samples, oxidized at 1200°C for 90 min. and at 1300°C for 1 min.

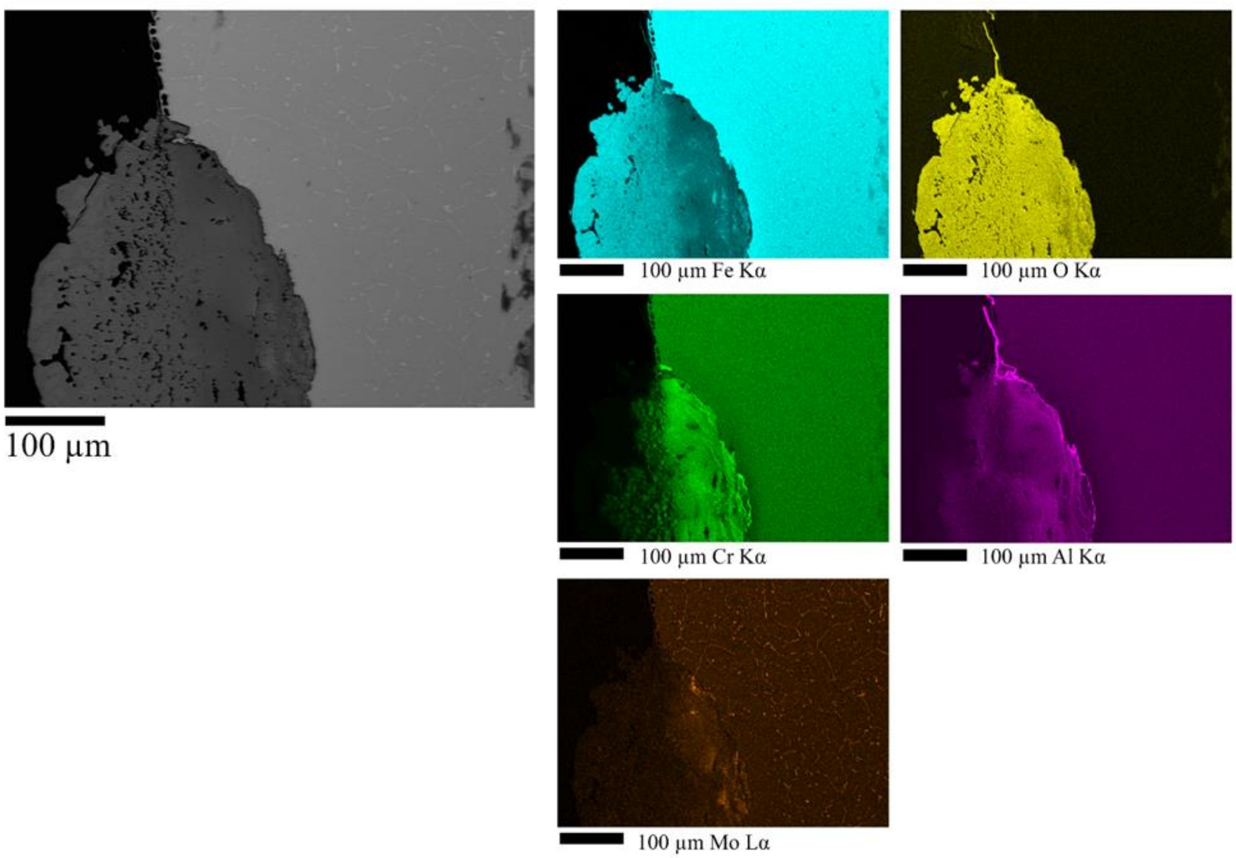

Figure 21. EDS maps showing the oxide beyond the original sample surface.